Polymer-based photonic integrated circuits

R. T. CHEN

A myriad of passive and active guided-wave devices has been successfully demonstrated using the photolime gel polymer. These include high density linear and curved channel waveguide arrays, electro-optic modulator and modulator arrays, highly multiplexed waveguide holograms for wavelength division demultiplexing and optical interconnects, waveguide lens, and rare-earth ion-doped polymer waveguide amplifiers. A single-mode linear channel waveguide array with device packaging density of 1250 channels cm^{-1} has been achieved. The first 12-channel wavelength division demultiplexer working at 830, 840, 850, 860, 870, 880, 890, 900, 910, 920, 930 and 940 nm on a GaAs substrate is also described in this paper. A polymer-based electro-optic travelling wave modulator with 40 GHz electrical bandwidth is further delineated. A rare-earth ion-doped polymer waveguide amplifier working at 1.06 μm with 8.5 dB optical gain is also achieved using this polymer matrix. The tunability of the waveguide refractive index of photolime gel polymer allows the formation of a graded index (GRIN) layer. As a result, these active and passive guided wave devices can be realized on any substrate of interest. High quality waveguides (loss <0.1 dB cm^{-1}) have been made on glass, $LiNbO_3$, fused silica, quartz, PC board, GaAs, Si, Al, Cu, Cr, Au, Kovar, BeO, Al_2O_3 and AlN.

KEYWORDS: guided-wave devices, polymers, integrated circuits, optical interconnects

Introduction

The development of advanced optical materials that can focus, modulate, multiplex, transmit, receive, demultiplex and demodulate optical signals, will be the key to the realization of economical and reliable wide band ($\sim$THz) optoelectronic systems for optical signal processing and computing applications. To date, efforts have focused on the development of hybrid and monolithically integrated devices and systems in the $LiNbO_3$ and III-V material systems, respectively. A number of technology-related issues, however, currently impede further progress. In particular, both $LiNbO_3$ and III-V semiconductors are incapable of producing the large index modulations that are required to create multiplexed phase gratings, which constitute one of several important building blocks in very large scale optically interconnected systems. Second, the requirements of lattice-matching have severely restricted the number, size and types of materials that can be grown on top of the III-V compound substrates and epilayers. Third, dielectric constants of these materials are dispersive and relatively high when compared with polymeric materials. These factors reduce the modulation bandwidth of electro-optic waveguide modulators. Lastly, device yields have been relatively low, while costs associated with the growth and processing of related microstructures have been high. Hence, the development of new, low-cost materials that can be processed into microstructural optical components, such as waveguides and gratings, will be invaluable to the future optoelectronic integration effort.

Due to the constraints of $LiNbO_3$ and III-V material systems, guided wave devices research has been concentrated on polymer-based materials. Polymer molecules are formed by combining a myriad of monomers. Therefore, by definition, an infinite number of polymers can be formed. The polymeric materials suitable for guided-wave device applications, in general, and specifically for optical interconnection are the ones that demonstrated acceptable optical and mechanical properties. Both passive and active polymer-based guided-wave devices have been demonstrated using different polymeric materials[1–20].

The author is at the Microelectronics Research Center, Department of Electrical and Computer Engineering, University of Texas at Austin, Austin, TX 78715, USA. Received 19 January 1993. Revised 18 May 1993. Accepted 25 May 1993. This paper was invited by the Editorial Staff of *Optics & Laser Technology*.

0030–3992/93/060347–19

In this paper, I report on the development and study of new polymer-based passive and active guided wave devices employing photolime gel. This is a non-synthesized superpolymer extracted from animal bones. It overcomes many of the problems associated with the fabrication of conventional microstructural thin-films, as described above, and shows promise for becoming a new building block in photonic circuit systems. Polymer microstructure waveguides (PMSWs), which exhibit low loss (0.1 dB cm^{-1}) (see Ref. 21) and excellent optical quality (low defect number), have been formed on a variety of substrates, including GaAs, $LiNbO_3$, glass, Al, Al_2O_3 and BeO.

Recent experimental efforts have also demonstrated PMSWs on Si, quartz, fused silica, phenolic PC board, Cu, Cr, AlN and Kovar. Optical waveguides with slab guiding layers as large as 50 cm × 50 cm have been constructed. In addition, the ability to control the refractive index profile of the guiding region, during the fabrication process, has been demonstrated. As a result of this refractive index profile tuning capability, it has been possible to fabricate low-loss polymer waveguide structures on any type of substrate, including semiconductors, conductors, insulators, and ceramics, regardless of the substrate refractive index and conductivity. A local sensitization technique, used in conjunction with the polymer films, has been developed to facilitate the formation of χ^2 non-linear polymer waveguide amplifier and multiplexed holograms. The results achieved thus far are summarized in Table 1 with the device features on $LiNbO_3$ and GaAs as references. Details of these polymer-based guided wave devices are addressed sequentially in this paper.

Formation of polymer microstructure waveguides

High quality thin polymer films, which exhibit propagation losses of less than 0.1 dB cm^{-1}, can be formed from pure photolime gel polymers. When the gel is first formed, it exists, in an aqueous solution, as a series of single polymer chains surrounded by adjacent water molecules. After standing for a period of time at temperatures below 30°C, solutions

Table 1. Demonstrated features of polymer-based integrated optical devices at the Microelectronics Research Center of the University of Texas, Austin with GaAs and $LiNbO_3$ devices as a reference

	Technology		
Features	Polymer-based	GaAs	$LiNbO_3$
1. Planar waveguide	Yes	Yes	Yes
2. Channel waveguide	Yes	Yes	Yes
3. Electro-optic modulator	Yes[a]	Yes	Yes
4. Waveguide propagation loss	<0.1 dB cm^{-1}	0.2 to 0.5 dB cm^{-1}	<0.1 dB cm^{-1}
5. OEIC size	Unlimited[b]	Limited[b]	Limited[b]
6. Forming of multiplexed grating	Yes[c]	No	No
7. Channel waveguide packing density (channels cm^{-1})	High[d]	High	High
8. Implementation of other substrates	Easy[e]	Difficult[f]	Difficult[f]
9. Large area multiple-guiding layer on single substrate	Yes	No	No
10. Waveguide lens	Yes	Yes	Yes
11. Dielectric constant dispersion	Low[g]	High	High
12. Potential modulation speed	>100 GHz[h]	~30 GHz	~30 GHz
13. Fabrication cost	Low	High	High
14. Mouldability	Yes	No	No
15. Waveguide amplifier	Yes	Yes	Yes

[a]Non-linear polymer with λ_{33} larger than $LiNbO_3$ and GaAs has been reported.
[b]Polymer can be implemented on any large substrate while GaAs and $LiNbO_3$-based OEICs are limited by the crystal dimension.
[c]High index modulation of the same polymer material allows us to multiplex hundreds of gratings on the same area for one-to-many fan-out (useful for high-speed clock signal distribution).
[d]Up to 1250 channels cm^{-1} on polymer 500 channels cm^{-1} on GaAs and 333 channels cm^{-1} on $LiNbO_3$ were reported.
[e]Thin film coating.
[f]By deflection GaAs and $LiNbO_3$-OEICs are thick film devices which are difficult to transfer to other substrates.
[g]Polymer dielectric constant is controlled by electron oscillation which has a very small dispersion from microwave to optical wave.
[h]Small dielectric constant dispersion gives very small walk-off between microwave and optical wave.

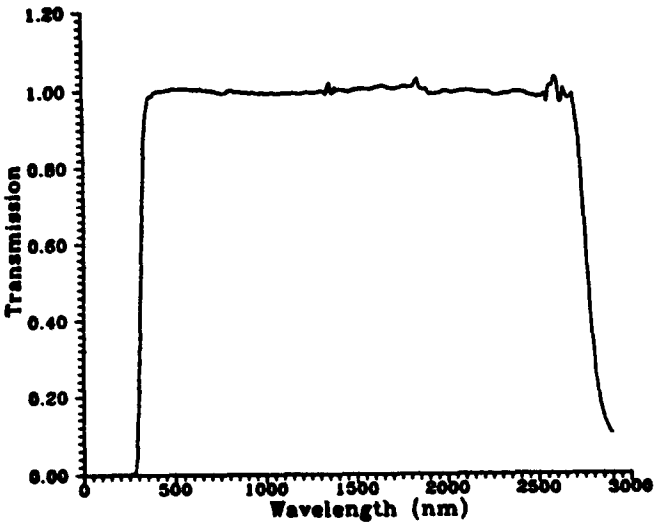

Fig. 1 Transmission bandwidth of the polymer thin film

containing more then 1% photolime gel solidify, forming films that are rigid, and, henceforth, rubber-like in their mechanical properties[21].

An optical thin film is formed from the pure photolime gel polymer by mixing solutions having various gel/water ratios, and spinning the solutions on top of a substrate material. By changing the gel/water ratio, or the spin speed of film coating, film thicknesses can be achieved that vary from less than 1 mm, to greater than 100 mm in dimension. The optical transmission characteristics of a 10 mm thick gelatin polymer film, formed in the above fashion, are shown in Fig. 1. It can be seen that the film is nearly 100% transparent from a wavelength of $\sim$300 nm to greater than 2700 nm. The above film properties were found to be relatively insensitive to temperature changes. In particular, recent experimental results indicated that the transmission and index properties are stable over the temperature range from -196°C to $+180$°C for dry films or holograms prebaked at $+180$°C (see Ref. 22).

Other tests, performed on the polymer films, have also indicated a high degree of immunity and radiation hardness to some nuclear and high power microwave radiation source[23]. In addition, films prepared in the above manner were previously shown to possess step index profiles[24,25]. Their formation on absorptive, or higher index, substrate materials would, therefore, result in the creation of leaky mode waveguides having excessive propagation loss. The influence of substrate loss on guided wave propagation behaviour was experimentally confirmed by depositing polymer films on top of Al_2O_3 and BeO ceramic substrates, respectively, and measuring the mode attenuation via a prism coupling technique. High losses, measured to be in excess of 40 dB cm^{-1}, make the step-index polymer films, as processed above, unsuitable for waveguiding applications. Ideally, the ability to change the index from a step, to a graded-index profile with a higher surface index, would enable polymer films to be used on low loss, as well as extremely lossy, substrate materials. In this case, the lower index portion of the graded index polymer films would function as a waveguide cladding layer. It would reduce the evanescent field overlap with the underlying substrate, and provide tighter mode confinement closer to the polymer film surface. In order to achieve low-loss waveguiding in the gel films, a method of tuning the refractive index profile from a step index to a graded-index profile was developed.

A combination of systematic wet and dry processing techniques was employed to perturb the mass density of the polymer and, hence, the polymer refractive index. The index of refraction of the newly perturbed polymer film can be qualitatively estimated using the Lorentz–Lorenz formulation[26], in terms of the average number of molecules, per unit volume, that possess different mass densities. The process of index tuning is actually one of controlled absorption and dehydration. The film is first hardened in a fixer solution, and then immersed in a de-ionized water bath. During this later step, water absorption causes the film to swell. The process is then reversed by dehydrating the polymer film in a temperature-controlled alcohol bath. In order to prevent film microcracking, the alcohol concentration is slowly and gradually increased during the final phase of processing. Qualitative data, not shown, but obtained from scanning electron micrographs, indicated that the polymer mass density decreases monotonically towards the substrate surface. Various refractive index profiles for multimode PMSWs, created through the index tuning method, were experimentally measured using the prism coupling technique, and analytically determined using the Inverse Wentzel-Kramers Brillouin (IWKB) method[27,28].

The results of these measurements and calculations are shown in Fig. 2 for polymer films that have been deposited on top of Al_2O_3, Al and GaAs substrates, respectively. Refractive index profiles were calculated by finding solutions to the eigenvalue problem, based upon a suitable application of the boundary

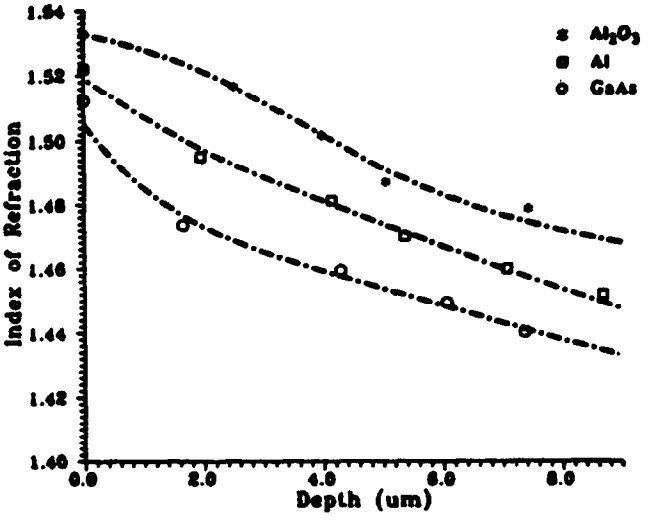

Fig. 2 Graded index profiles of Al_2O_3, Al and GaAs determined by the IWKB method

conditions at the waveguide surface. The WKB approximation then yields, as a function of the depth parameter h, the following integral expression for the polymer refractive index[26]

$$\int_0^{h_q} (N^2(h) - N_{\text{eff}_q}^2)^{1/2}\, dh = \frac{4q-1}{8} \quad q = 1, 2, \ldots \qquad (1)$$

Here, h is normalized to the free space wavelength λ. h_q is defined by the relation $N(h_q) = N_{\text{eff}_q}$, $h_0 = 0$, $N_{\text{eff}_0} = N(0)$, and the integral is performed over the extent of the polymer film. The above expression provides an accurate treatment in the present case, since the effective index of the zeroth order mode, within the multimode waveguide, is very close to that of the waveguide surface index. As seen in Fig. 2, a number of different tuned index profiles can be achieved, through careful control of the polymer absorption and dehydration process. We note that the profile variations on the three different substrates result from differences in process parameters, rather than from substrate-related dependences. In all cases, a reduction in the overlap between the guided mode evanescent field and the underlying substrate, due to the presence of a graded index profile, resulted in the observation of strong waveguiding and propagation losses of 0.1 dB cm^{-1} in the PMSWs.

Low loss waveguiding is also depicted in Fig. 3 for polymer films deposited on Si, quartz, Au, and Al_2O_3, respectively. Similar results have been observed for polymers deposited onto other substrate materials, including Si, $LiNbO_3$, fused silica, Al, Cu, Cr, Kovar, BeO, AlN and phenolic PC board, respectively. Without the use of special adhesion promoters or surface planarizing layers, the majority of polymer films displayed excellent deposition and adhesion properties on most of the substrates described above. There are no observed effects on the substrate materials, described above, due to the presence of the polymer layer and the associated chemical processing techniques.

Formation of linear and curved channel waveguide array

In this section, we report the cross-link induced linear and channel waveguide arrays on graded index

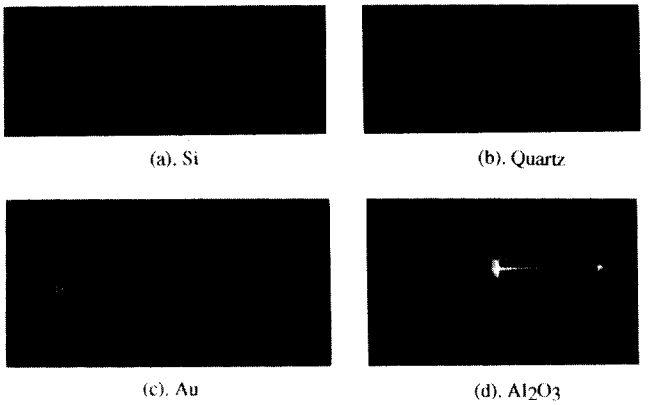

Fig. 3 Graded index polymer microstructure waveguide on Si, quartz, Au and Al_2O_3

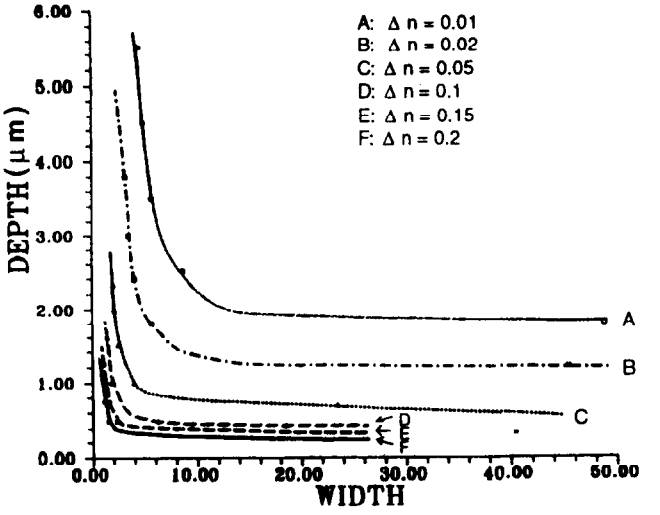

Fig. 4 Single-mode polymer channel waveguide dimension based on the effective index method with index modulation as a parameter

(GRIN) photolime gel[21,30]. The GRIN characteristic of the polymer thin film allows us to implement such a channel waveguide on any substrate of interest. After the polymer film was spin-coated on a substrate, it was dipped into ammonia dichromate solution for sensitization. Formation of a channel waveguide was realized by cross-linking the polymer film through ultra-violet exposure. It was observed that the cross-linked area has a higher index of refraction than the unexposed area. The index modulation due to the photo-induced cross-link can be as high as 0.2 (see Ref. 31). Consequently, the channel waveguide confinement and thus the packaging density (number of channels cm^{-1}) can be extremely high.

Implementation of the waveguide pattern was realized either by laser beam direct writing or through a conventional lithographic process. The graph in Fig. 4 was produced by computer simulation based on the effective index method[32]. It shows the optimal single-mode channel waveguide dimensions for an optical wavelength of 1.31 μm. The cut-off dimension is shown with index modulation as a parameter. Note that the cut-off boundary defined here is for E_{12}^x (see Ref. 33) above which the channel waveguide becomes multimode. (E_{ij}^x denotes the ijth mode with the major electric field along the x direction). Marcatili's five-region method was also used for this purpose. The result (not shown) is very close to that of Fig. 4. However, the cut-off dimension for E_{11}^x determined by the effective index method[29,30] is quite different from that determined by Marcatili's method. In any case, the waveguide cut-off dimension for E_{12}^x is well above the cut-off condition for E_{11}^x. The discrepancy between these two methods for E_{12}^x is negligible.

The experimental results of a linear polymer channel waveguide array working at 0.63 μm and 1.31 μm were experimentally verified using the set-up shown in Fig. 5(a). A microprism was employed[34] to provide simultaneous coupling for multiple channels. The observed near-field patterns for 0.63 and 1.31 μm, using the set-up shown in Fig. 2(a), are displayed in

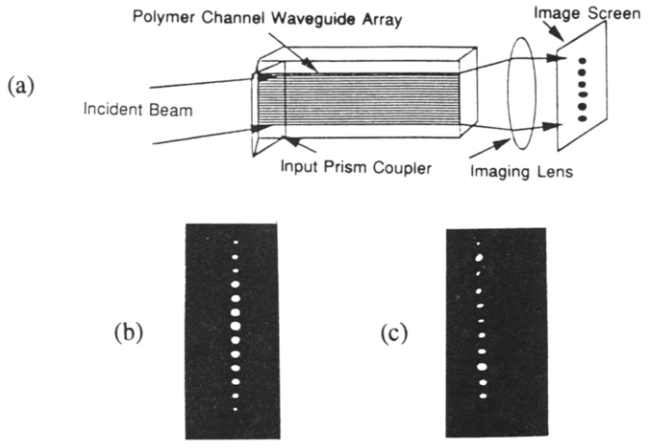

Fig. 5 (a) Experimental set-up for the observation of polymer channel waveguide array (channel width = 2 μm), and near-field patterns of the channel waveguide array for wavelengths at (b) 0.63 mm and (c) 1.31 mm, respectively. The channel separation is 8 μm

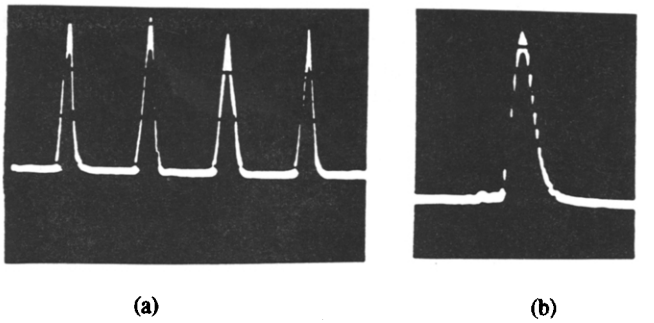

Fig. 6 Mode profile of the single-mode channel waveguide array in (a) the horizontal (peak-to-peak separation is 8 μm) and (b) vertical directions

Figs 5(b) and 5(c), respectively. A single-mode waveguide at 0.63 μm was further confirmed by employing a Si charge-coupled photodetector (CCPD) array to image the mode profile in both horizontal and vertical directions. The packaging density of the waveguide device shown in Figs 5 and

wiring for board-to-board interconnections. Confirmation of single mode guiding at 0.63 μm assures that the waveguide mode for 1.31 μm shown in Fig. 5(c) is also single-mode[35].

To provide optical interconnects on the intra-MCM (multi-chip module), inter-MCM and backplane levels, an optical bus may need to be curved in order to transmit optical signals to the addressed location (for example, memory). To evaluate the feasibility of generating a curved polymer waveguide, channel waveguides with radii of curvature (ROC) from 1 mm to 40 mm were made. Table 2 summarizes the parameters of the curved waveguides fabricated. Large index modulation caused by photo-induced cross-linking provides a better waveguide confinement factor and thus a smaller ROC. Theoretically, the loss due to waveguide bending can be negligibly small if[36]

$$\mathrm{ROC} > \frac{3N_{\mathrm{eff}}^2\lambda}{\pi[N_{\mathrm{eff}}^2 - N_c^2 + (\lambda/2b)^2]^{3/2}} \qquad (2)$$

where N_{eff} is the guided wave effective index, N_c is the cladding layer index and λ and b are the optical

wavelength and the width of the channel waveguide (see the inset in Fig. 4). Note that in deriving (1), the wave-number of the guided wave along the x direction is assumed to be equal to $\lambda/2b$.

Figures 7(a), (b) and (c) show the experimental results of a curved polymer channel waveguide. The coupling angle of the input prism was set at the phase matching angle for E_{11}^x mode. No surface scattering can be observed from the image taken by a vidicon

surface (Fig. 7(a)). A bright spot was observed. The bright streak on the waveguide surface which can be an indicator of loss[34], disappeared (Fig. 7(a)) in our linear and curved channel waveguide devices. The photograph shown in Fig. 7(b) is the linear field mode pattern at the output end of the curved channel waveguide using end-face imaging. Special surface treatment is needed to increase the loss and thus make surface scattering visible. Fig. 7(c) shows a curved waveguide with the same pattern of Fig. 7(a) after surface treatment.

The value of the index modulation plays an important role in minimizing the propagation loss for the curved region. The larger the index modulation, the better the waveguide confinement factor. The evanescent field decays drastically in the cladding region. The radiation loss due to velocity mismatch[36,37] is thus minimized. As far as the waveguide propagation loss is concerned, the measured loss in the neighbourhood of 0.1 dB cm^{-1} has been consistently observed. Purification of the polymer thin film significantly reduced

Table 2. Curved waveguide parameters under investigation

Channel width (μm)	Radius of curvature (mm)	Degrees of rotation
10	1	90, 180
10	2	90, 180
10	3	90, 180
10	4	90, 180
10	4.5	90, 180
10	40	90, 180

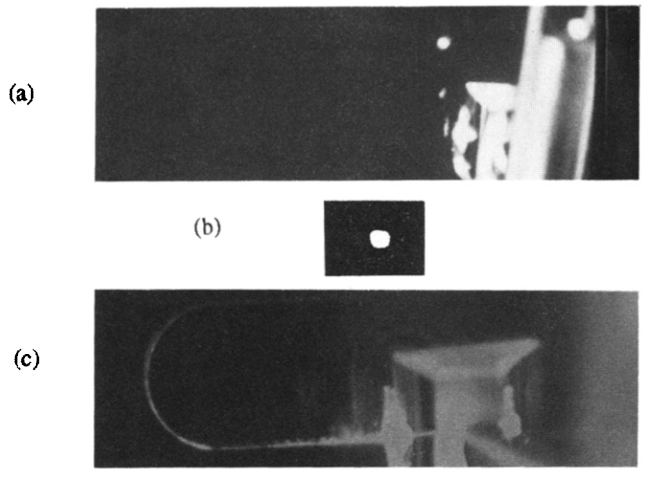

Fig. 7 Experimental results of curved channel waveguides. (a) Observation of a curved channel waveguide (ROC = 3 mm) at the scribed waveguide surface, (no surface scattering can be observed); (b) near-field pattern of the curved channel waveguide with the same ROC of (a); (c) observation of the curved channel waveguide with a ROC equivalent to that of Fig. 7(a) after surface treatment

the volume scattering centres within the guiding medium.

The advancement in high-speed computers requires an interconnection technology capable of routeing high-speed signals, especially clock distribution for a synchronous bus such as NUbus[38] and high speed data for a compelled asynchronous bus such as VMEbus and Futurebus[38].

Electrical interconnects using either thin metal films or transmission lines are not efficient enough to provide highly parallel, high-speed (> 1 GHz) connections for distances longer than 1 cm. Optical interconnections based on polymer waveguides have been reported to provide two-dimensional (2-D) and three-dimensional (3-D) optical interconnects with 60 GHz modulation bandwidth and 22 dB signal-to-noise ratio[39]. The results presented here give us a package density as high as 1250 channels cm^{-1} with a propagation loss as low as 0.1 dB cm^{-1}. For computing systems using hypercube, daisy chain and star interconnect architectures, the single layer optical interconnects reported here are sufficient to provide the required interconnectivity. Implementation of fibre arrays for current backplane buses such as VMEbus and Futurebus is not practical since these bus architectures connect all processor and memory cardboards in parallel, along a set of common communication lines which can, in general, be driven by any machine and listened to simultaneously by all machines (for example, using low efficiency coupling holograms). Thus, any machine on a bus can communicate directly with any other (subject to bus ownership protocols). As a result, implementation of a practical optical backplane bus requires a microlithographic process which is not applicable for fibre arrays. Furthermore, the GRIN property of the polymer waveguide facilitates the implementation of optical integrated circuits on any optoelectronic substrate.

Formation of waveguide holograms by local sensitization with applications to WDM

The formation of tuned index polymer waveguides, on virtually any kind of substrate, as described above, provides the basis for the development of other passive and active optical devices which are suitable for signal routeing and modulation. In particular, devices which utilize multiplexed holograms, for wavelength multiplexing and demultiplexing operations, are key components for advanced optical interconnection architectures. Based upon the refractive index tuning capability within the polymer film, microlithographic techniques were used, in conjunction with a local sensitization process, to generate waveguide multiplexed holograms. After the polymer film was deposited and cured on top of a suitable substrate, a photoresist window was defined using standard photolithography. Local sensitization was then achieved by immersing the selectively-masked sample into a room-temperature ammonia dichromate solution[40]. The masking material was then removed and, within two hours after drying and stabilization of the sensitized region, the sample was ready for holographic recording and processing.

A similar process was used to form multiplexed holographic phase gratings in the PMSW films. The gratings were created by successively exposing holographic patterns within the selectively defined and sensitized regions of the waveguide. A two-beam intereference recording method was used to define individual holographic gratings, each at a different recording angle, and each having a sinusoidal phase modulation profile, such that

$$K_i = 2k_{\lambda_i} \sin\left(\frac{\alpha_i}{2}\right) \tag{3}$$

where k_{λ_i} and K_i are defined as

$$k_{\lambda_i} = N_{\text{eff}_{\lambda_i}} \frac{2\pi}{\lambda_i} \tag{4}$$

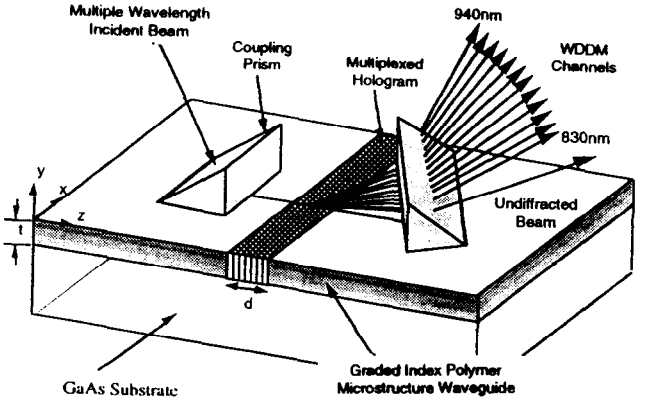

Fig. 8 A schematic of the locally sensitized polymer waveguide, containing a multiplexed holographic phase grating

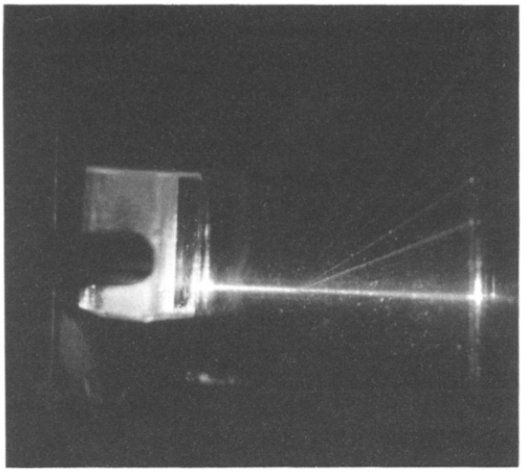

Fig. 9 Four-channel polymer waveguide wavelength division demultiplexer working at 632.8 nm (red), 611.9 nm (orange), 594.1 nm (yellow) and 543.0 nm (green)

and

$$K_i = \frac{2\pi}{\Lambda_i} \tag{5}$$

Here, α_i is the angle of Bragg diffraction, Λ_i is the ith holographic grating period, K_i is the ith grating wavevector, and $N_{\text{eff}_{\lambda_i}}$ is the waveguide mode effective index at λ_i. The resultant grating wave vector for each hologram lies within a plane that is parallel to the waveguide surface. A schematic of the locally sensitized polymer waveguide, containing a multiplexed holographic phase grating, is depicted in Fig. 8.

The above technique was used to develop a four-channel wavelength division demultiplexer (WDDM) that operates at the centre wavelengths of 632.8 nm (red), 611.9 nm (orange), 594.1 nm (yellow), and 543.0 nm (green), respectively. The device consisting of a locally-sensitized single-mode PMSW, and prepared on a Soda-Lime glass substrate, is shown in Fig. 9. Only the TE_0 guided mode of the waveguide is excited via the prism coupler, and utilized in the present device. Holographic recording angles, for each of the deflected wavelengths, were chosen, commensurate with the effective index dispersion relations of the polymer film. The Bragg diffraction angle of each resulting transmission phase grating was designed to satisfy the phase-matching condition for the signal wavelength of interest. Exposure parameters were adjusted during successive holographic recordings, in an attempt to optimize diffraction efficiencies. Each grating was, therefore, designed to be capable of deflecting only one wavelength within a 4–10 nm spectral bandwidth. Device measurements yielded a crosstalk figure of less than -40 dB between adjacent channels, and a corresponding diffraction efficiency of better than 50% at each wavelength. The angular and spectral sensitivities for the demultiplexer were theoretically determined to be within 0.2°–0.4°, and ~4–10 nm, respectively. It is expected that even higher diffraction efficiencies, for each grating, can be achieved, if the grating modulation index and the interaction length are optimized accordingly.

In addition, while excellent crosstalk figures were obtained for the present waveguide demultiplexer, it is conceivable that the presence of substrate radiation modes from each signal carrier, generated by the interaction with other existing gratings, will limit the overall device efficiency for closely spaced channels. These modes might be present as a consequence of random fluctuations in the grating modulation index and waveguide thickness, or from variations in the tuned refractive index profile.

A 12-channel WDDM device was further demonstrated on a semi-insulating GaAs substrate[41]. The gratings were designed to operate at the diffraction angles of 10, 15, 20, 25, 30, 35, 40, 45, 50, 55, 60 and 65 degrees to disperse selectively signals at the centre wavelengths of 830, 840, 850, 860, 870, 880, 890, 900, 910, 920, 930 and 940 nm, respectively. For each λ_j, the corresponding recording angles were selected to generate a waveguide transmission hologram with the desired grating periodicity. The interaction length of the multiplexed waveguide hologram is 0.4 mm. The mode dots coupled out of the prism coupler are shown in Fig. 10 with the corresponding wavelengths as indicated. The observation of these clean mode dots verified the quality of the polymer waveguide. A proportion loss in the neighbourhood of 0.1 dB cm^{-1} has been routinely achieved in a Class 100 clean room environment.

The noise of the fan-out channels of the WDDM device is mainly from the crosstalk of the signals from adjacent channels. An average crosstalk figure of -20.5 dB was measured with diffraction efficiency from 40% to 55% among these output channels. The spectral width of the $Ti:Al_2O_3$ laser from Spectrophysics was also measured. A -3 dB bandwidth of ~4 nm was found. The results suggest that the WDM devices of better than 4 nm wavelength separation cannot be experimentally ralized without significant channel crosstalk. Theoretically, our device structure is capable of operating at a channel-to-channel spacing as small as 1 nm under the current design when a DFB laser

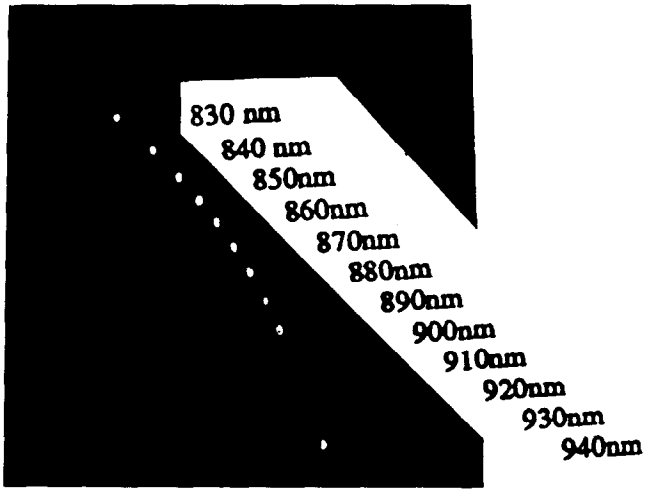

Fig. 10 12-channel WDDM on a semi-insulating GaAs substrate

diode is employed. The −20.5 dB crosstalk is primarily due to the wavelength spreading of the $Ti:Al_2O_3$ laser rather than the waveguide device itself.

As far as the throughput intensity is concerned, the 33% diffraction efficiency represents an output power as high as 50 mW. For a communication system involving the reported WDDM device, the system power budget will be determined by laser power, modulation speed, bit error rate and detector sensitivity. Employing a PIN-FET as the demodulation scheme, theoretically we can utilize a ~0.5 Mw semiconductor laser to obtain 1 Gbit s^{-1} communication with a 21.5 dB signal-to-noise ratio. The above power budget assumes 50% diffraction efficiency, 1 dB waveguide propagation loss, 3 dB waveguide coupling loss, 2 dB hologram excess loss, 4 dB fibre propagation loss, 5 dB system power margin and room temperature operation condition with an amplifier noise figure equal to 4. The current design allows us to providc 60-channel multiplexibility with the maximum value of index modulation set at 0.1.

X^2 electro-optic polymer

Gelatin is a class of biopolymer which consists of thousands of 10–20 Å long amino-acids. Gelatin has been classified as a superpolymer[42] because of its extraordinary chemical and physical properties and its molecular structure. The remarkable fact is that biological gelatin has two extraordinary microstructural morphologies: (1) two dimensional network—molecules are partially aligned and cross-linked with interchain hydrogen bonds to form a helical collagen-like sheet (Fig. 11); and (2) thermoplastic→thermosetting—the processible gelatin (thermoplastic form) can be readily transformed into a highly cross-linked and insoluble polymer (thermosetting form) using heat or ultra-violet radiation curing.

When gelatin is incorporated with ammonia dichromate, it becomes a widely used holographic

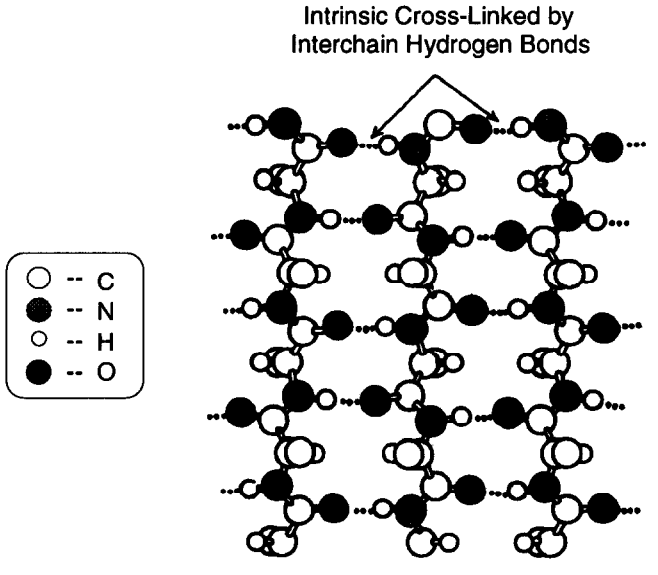

Fig. 11 The sheet-like structure of photolime gel with intrinsic crosslinking

recording material; dichromate gelatin (DCG). Holographic gelatin has attracted a great deal of interest because it has a variety of applications. Incorporation of different guest molecules significantly change the electro-optic properties of the polymer matrix. Such a material characteristic motivates us to develop further X^2 non-linear polymers using non-linear dye/photolime gel combinations.

The search for materials with fast response times (<1 ns), combined with a large electro-optic (EO) effect ($\Delta n > 10^{-4}$), and which are simple to process has been of intense interest for some time. EO materials, such as liquid crystal, photorefractive and piezoelectric materials, offer large EO effects but exhibit a switching time which is too slow (50 ns–ms) for practical applications. Also, the widely used inorganic crystalline ($LiNbO_3$) thin film is very difficult to process. In contrast, EO polymers offer excellent properties, including large EO coefficients ($\Delta n \cong 5 \times 10^{-4}$), low-temperature processing (<200°C), and fast response times (<300 ps). In recent years, EO poled polymers have evoked international attention and effort. High glass transition temperture (T_g) polymers or cross-linked polymers have proved their effectiveness for stability enhancement. Unfortunately, their long-term EO stability is still a bottleneck for practical device applications[43]. While tremendous efforts have been put into the characterization of poled materials[44], device research on EO polymers is still in its infancy. For the most part, this is due to the fact that the basic criteria for guided wave materials is that they have the capability to be integrated with other optoelectronic components. At present, this aspect of most EO polymers has not been examined. Polymeric gelatin has been proved to be an excellent material for the fabrication of an array of guided wave optical elements, but no active EO device has been built in the gelatin media. The purpose of this section is to describe the achievement of assembling an EO modulator by the incorporation of active EO materials in the highly crosslinked gelatin matrix.

The gelatin used in this experiment is known as type A gelatin, acid-treated protein derived from animal tissues. It has an isoelectric point between pH 7 and pH 9. Gelatin is soluble in aqueous solutions and insoluble in most organic solvents, such as benzene, acetone, petroleum ether and absolute alcohol. This low solubility limits the use of a large number of EO dyes which are frequently water insoluble. In the experiment described here, 4-nitrophenol (NP) from Aldrich was selected as the active EO material. Nitrophenol has very high solubility in water (25 mg ml^{-1}) and can homogeneously disperse in gelatin matrix. The electron acceptor NO_2 group and electron donor OH group form a linear dipole moment across the p-conjugated electronic system. The molecular non-linear hyperpolarizability of NP in solution has been gauged to be about 1/3 that of methyl nitroaniline (MNA) by measuring the electric field induced second harmonic generation[43].

A solution containing polymer gelatin (30 g), nitrophenol (~20 to 30% by weight), and water

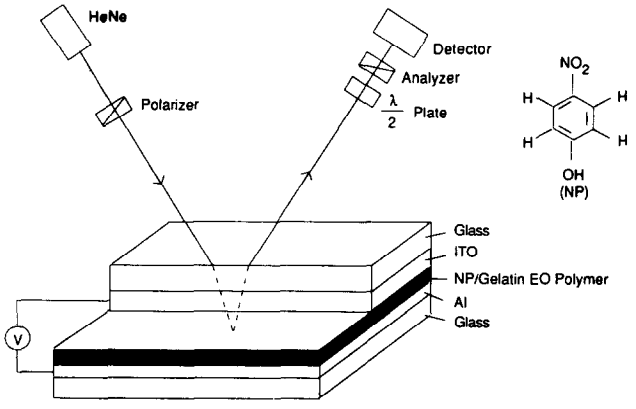

Fig. 12 Electro-optic measurement set-up

(400 ml), was set in a water bath (60°C) until it became clear. The solution was filtered and spin coated on an aluminium (Al)/glass substrate. The absorption peak of NP is at 304 nm. It has a very wide optical bandwidth, from 350 nm to 2700 nm, which is much wider than most EO polymers. From the interference fringe, the thickness of the thin film was measured to be 10 μm. The thickness of polymer thin films can be varied from submicron to 100 μm by changing the ratio of water and gelatin or the speed of spin-coating. The dry thin film was covered with an optically transparent indium tin oxide (ITO)/glass substrate. The Al and ITO electrodes served as poling fields as well as modulating fields. Although gelatin molecules are partially aligned microscopically, no macroscopic birefringence was found in the gelatin film before poling. The poling and curing processes were performed at the glass transition temperature (T_g), 60 to 70°C, for 30 minutes.

The experiment was performed in the reflection geometry[44] (see Fig. 12) with a 3 mW HeNe laser beam polarized at 45° to the plane of incidence, so that the parallel and perpendicular components of the optical field were equal in amplitude. The beam reflected from the Al coating was propagated through a half-wave plate, an analyser and into a photodiode. The anlayser was set at a cross-polarization angle with respect to the polarizer. The half-wave plate was used to generate $\pi/2$ phase retardation between x and y polarizations of the laser beam. When the phase shift, ψ, is biased at $\pi/2$ with a $\lambda/2$ plate, the output intensity is approximately linearly related to the phase retardation as well as to the applied modulating voltage. The ratio between the modulated intensity, I_m, and the DC signal, I_c, can be expressed as

$$I_m/I_c = (2p/\lambda) \times 2d \times \Delta n \times (\sin^2\theta/\cos\theta) \quad (6)$$

where θ is the angle of incidence, d is the thickness of the polymer film, and Δn is the birefringence introduced by the modulation field. I_c is the output intensity at $\pi/2$ phase shift. This intensity can be obtained by rotating the $\lambda/2$ plate. This birefringence is given by

$$\Delta n = 1/2(n_3^3 \times \gamma_{33} - n_1^3 \times \gamma_{31})V/d \quad (7)$$

where n_1 and n_3 are refractive indices along the directions perpendicular and parallel to the poling electric field, respectively. For an initially isotropic system, the corresponding EO coefficients for light polarized perpendicular and parallel to the surface plane are related to γ_{31} and γ_{33}, $\gamma_{33} = 3\gamma_{31}$. This assumption can be justified because nitrophenol is randomly dispersed in the polymer matrix. Therefore, we have

$$\gamma_{33} = 3\lambda I_m \cos\theta/4\pi(n^3)V_m I_c \sin^2\theta \quad (8)$$

where V_m is the modulating voltage. The electro-optic effect of NP/gelatin polymer was observed with a poling field of 400 V across a 10 μm thick film. The optical modulation signal from a HeNe laser was displayed on an oscilloscope (see Fig. 13). The upper curve is 3.3 MHz RF modulation with a V_{p-p} of 90 V. The bottom curve is the corresponding modulated optical signal. Based on (8), the EO coefficient of NP/gelatin, γ_{33}, of 10–40 pm V^{-1} was obtained at 632.8 nm with a direct current. The spread in EO coefficient is due to variations in film thicknesses, dye concentrations, and poling fields.

The index change introduced by the modulation field is $1\text{–}4 \times 10^{-4}$. This value is comparable with many poled polymers and inorganic $LiNbO_3$. The major reason for the large non-linear effect is the high concentration of EO moieties, 35% by weight of NP, that can be incorporated into the gelatin matrix without any cluster appearing. This concentration is much higher than that in most guest/host systems ($\sim$15%). Effective poling may account for additional EO enhancement. For guest/host systems, the typical poling efficiency is between 10 and 20%. Poling efficiency for short-axis molecules, such as NP, is believed to be higher. This is because the short-axis molecule is subjected to a smaller axial force potential. Thus, the molecules can be rotated and aligned more easily.

The thermal stability of the poled EO response has been a critical issue in the practical application of poled polymers. The high T_g and crosslinked polymers have been used to reduce the diffusion of EO groups, and thus increase the thermal stability. The typical EO decay curve of guest/host polymers shows an initial fast decay to 20% within five days,

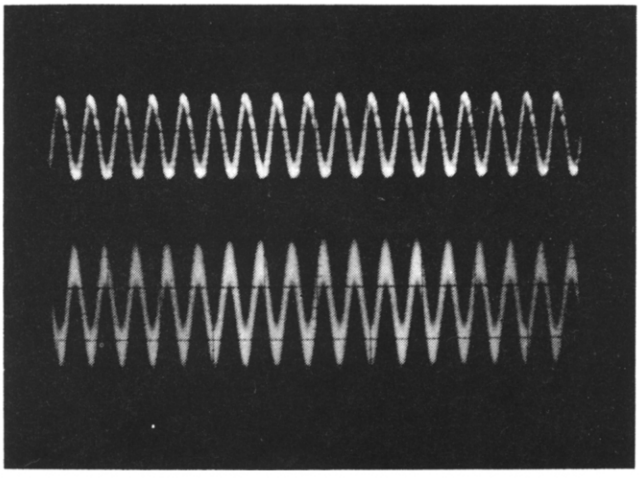

Fig. 13 The optical signal from a HeNe laser is modulated and displayed on an oscilloscope

followed by a slower decay. The EO stability of NP/gelatin shows that 40% of the original birefringence persists five days after poling at room temperature. As shown in Fig. 11, gelatin has two-dimensional sheet-like structures held by intermolecular hydrogen bonds.

During the thermal curing process, these chemical bonds in NP/gelatin can be further crosslinked and enhanced to form a rigid and irreversible thermosetting polymer. The observed results indicate that the highly crosslinked hydrogen bonds are responsible for the EO stability. In addition to the above intrinsic crosslinking, it is known that gelatin can be hardened and rendered insoluble by crosslinking between chromium ions and amino acid groups (in DCG) into a more stable three-dimensional network. We are currently characterizing the stability enhancement by crosslinking the poled gelatin with dichromate under exposure to laser radiation.

We have successfully constructed and demonstrated an EO modulator in biopolymeric gelatin. Nitrophenol was chosen as the active EO moiety and was shown to have a large EO effect. The planar structure of the gelatin plays an important role in the stability of the EO group in the polymer matrix. Optical birefringence was generated with a poling field at temperatures between 60° and 70°C. The results illustrate that active EO devices can be integrated into holographic gelatin films.

Rare-earth ion-doped (REI) polymer waveguide amplifier

During the past five years, intense research on single-mode rare-earth doped-fibre lasers and amplifiers has led to the development of a range of active devices, in particular the Er^{3+}-doped fibre amplifiers with applications for optical telecommunications at 1.5 to 1.6 μm. Integrated optics may offer an alternative way for realizing such single-mode waveguide active devices with potential advantages over fibres. These include compactness in size, feasibility of Q-switching, frequency doubling and the possibility of processing many devices on a single substrate. It also offers possibilities for new monolithic laser or amplifier components combining the medium's gain and the large range of integrated optical functions already demonstrated.

In this section, a Nd^{3+}-doped polymer waveguide amplifier is reported. All the demonstrated graded

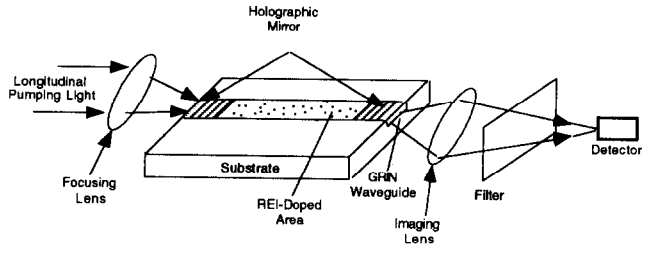

Fig. 14 Schematic of REI-doped polymer waveguide laser/amplifier

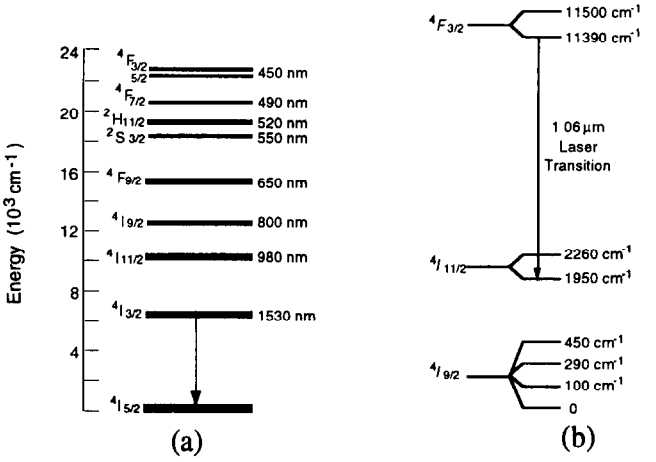

Fig. 15 Energy levels of (a) Er^{+++}-doped and (b) Nd^{+++}-doped glass waveguides. Metastable states and the corresponding stimulated emission lines are shown

index (GRIN) polymer waveguide devices reported thus far are summarized in Table 1. These devices include planar waveguides (1), channel waveguides (2), EO modulators (3), multiplexed gratings (6), multiple guiding layers (9), waveguide lenses (10) and waveguide amplifier (13). It is clear from Table 1 that all the guided wave elements made on $LiNbO_3$ and GaAs substrates can be replaced by polymer-based devices. More importantly, however, waveguide devices such as highly multiplexed gratings (6) and large area multiple guiding layers (9) can be realized only by using polymer-based technology. Formation of high efficiency holograms are important for the realization of the proposed architecture (Fig. 14). Each individual building block shown in Fig. 14 has been successfully developed and all the results can be found in the cited references.

Most of the waveguide lasers recently reported are Er^{+++}-doped lasers, primarily due to the 1500 nm lasing band. Depending on the wavelength of stimulated emission, the energy levels of Er^{+++}- and Nd^{+++}-doped glass waveguides labelled with the dominant Russel–Saunders ^SL_J term are shown in Fig. 15.

The Nd glass laser is a well known four-level system ($^4F_{3/2}$, $^4I_{11/2}$). The lasing action occurs between the metastable state $^4I_{13/2}$ to $^4I_{15/2}$ for Er^{+++}-doped glass waveguides. The fluorescence of higher states is almost fully quenched by the process of non-radiative multiphonon relaxation[45] which has a rate of more than 10^5–10^7 s^{-1}. The performance of waveguide lasers and amplifiers is governed by the relevant electronic and optical characteristics of active ions, such as cross-sections, spectral shapes of excitation and absorption bands, lifetime at the metastable state and their immunity to concentration quenching.

The host material has an important influence on all these properties. Note that the observation of Nd^{+++}- and Er^{+++}-doped waveguide amplifiers working at 1.06 and 1.50 μm, respectively, on various waveguide substrates, such as glass (amorphous state) and $LiNbO_3$ (single crystal), implies that the associated metastable states do exist in various host materials.

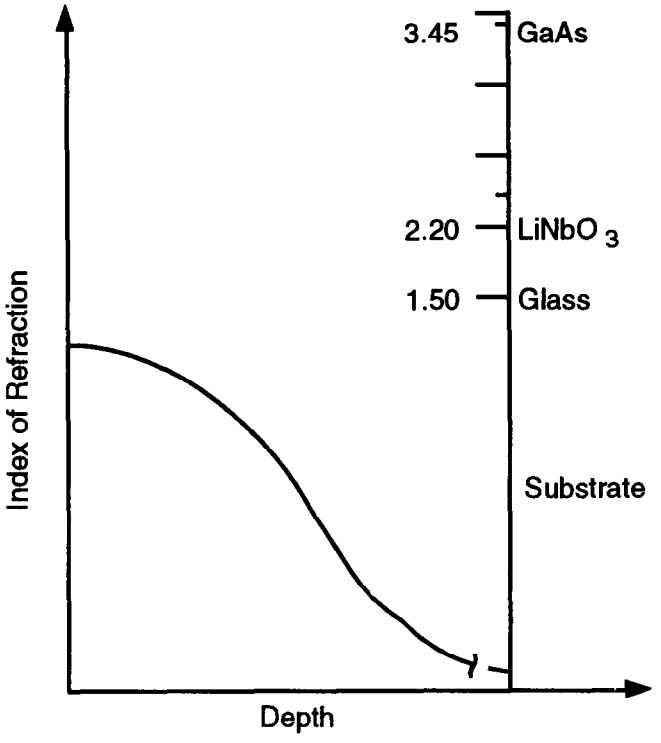

Fig. 16 Graded index profile of the polymer waveguide (this characteristic provides us with a universal method of implementing a waveguide laser on any substrate of interest (Table 3))

The polymer introduced is soluble in water. As a result, the chemical compounds containing REIs can be mixed with the host polymer as long as they are also soluble in water. The concentration shall be below the level of microscopic clustering which quenches the active ions.

Fluorescence lifetimes for $^4I_{3/2}$ for various glasses are 10^{-2} s (except for borate). There are certain concentration quenchers that basically shorten the lifetime of metastable states. The most serious quenchers are the admixed O-H groups whose concentration must be less than $3–5 \times 10^{18}$ cm^{-3} (see Ref. 46) for a glass waveguide amplifier. The existence of O-H groups generates a number of intermediate states between $^4I_{13/2}$ and $^4I_{15/2}$ (see Ref. 47). Such states, primarily from water molecules, significantly reduce the lifetime of the metastable state $^4I_{13/2}$. The general rule of thumb is that the lifetime of the excited state will be temperature dependent if the gap is less than ten times the effective phonon frequency and completely quenched if less than four times[47]. The water molecules within the photolime polymer can be totally eliminated using the dehydration process. Such a dehydration process provides us with not only an H_2O-free graded index (GRIN) polymer waveguide, but also a much higher temperature dynamic range (−100°C to 180°C) which ensures devices survivability under intense pumping situations.

The elimination of the excited state absorption (ESA) of pumping photons (for example, the $^4I_{13/2} > {}^4S_{3/2}$ transition) in an Er^{+++}-doped sample is always a potential problem. In three-level lasers, for there to be a gain in the first place, a significant fraction of the doping population must reside in the upper laser level. It is feasible to reduce the effects of ESA by detuning the pump wavelength away from the centre of the ground-state absorption feature[48]. The lasing level terminates at a thermally populated level above the ground state, and the laser therefore behaves as a quasi-four-level system. Consequently, the inherent loss of a waveguide laser is reported[48] to be reduced as the lasing wavelength is increased.

The host material, that is, photolime polymer gel, is an excellent guiding medium due to its wide transmission bandwidth (300 nm to 2700 nm). The graded index (GRIN) characteristics of this material (Fig. 16) allow the formation of high quality (loss < 0.1 dB cm^{-1}) single-mode devices on an array of substrates, as shown in Table 3. The wet processing method[12] used for profile tuning can also serve the purpose of O-H group quenching. The formation of a waveguide laser cavity is realized by recording two reflection holograms at the two end faces (Fig. 14) of the waveguide. The hologram fabricated is similar to a Lippmann hologram made for laser goggles which has an optical density (OD) of up to 6×10^{-6}. We have demonstrated waveguide transmission holograms by locally sensitizing the emulsions[49]. By changing the recording geometry, a reflection waveguide hologram can easily be made for this purpose.

For the three-level laser system, the equation governing the laser action is given by

$$\frac{\partial n_1}{\partial t} = \left(n_2 - \frac{g_2}{g_1}\right) c\phi\sigma + \frac{n_2}{\tau_{21}} - W_p n_1 \tag{9}$$

and

$$\frac{\partial n_2}{\partial t} = -\frac{\partial n_1}{\partial t} \tag{10}$$

In deriving (10), $n_{tot} = n_1 + n_2$ is assumed. In (9) and (10), n_1 and n_2 are the population densities of the upper and lower levels corresponding to the lasing wavelength, respectively. $g_1$and g_2 are the associated degeneracy, c is the speed of light in the medium,

Table 3. Substrates upon which graded index (GRIN) polymer waveguides have been demonstrated

Semiconductors	Si
	GaAs
Insulators	Glass
	$LiNbO_3$
	Quartz
	Fused silica
	Plastic thin film (PC Board)
Conductors	Aluminium
	Chromium
	Gold
	Copper
	Kovar
Ceramics	Al_2O_3
	BeO
	AlN

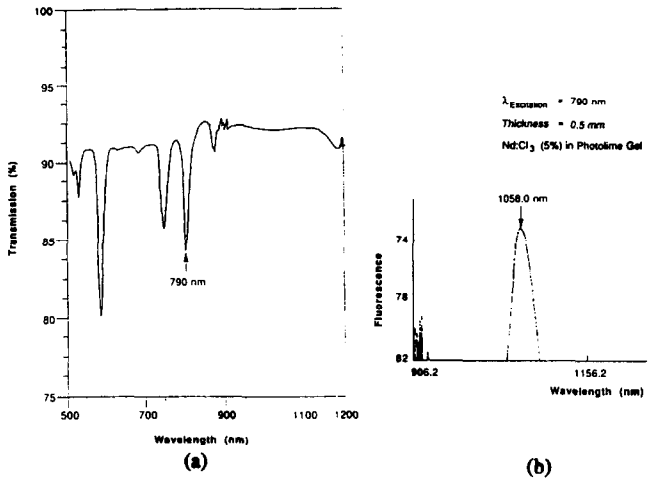

Fig. 17 (a) Absorption spectrum of the Nd^{+++}-doped polymer film, (b) fluorescent spectrum of the Nd^{+++} -doped polymer film

ϕ is the photon density (photons cm^{-3}), σ is the stimulated emission cross-section, t_{21} is the mean lifetime of the metastable state ($^4I_{13/2}$ for an E^{+++}-doped waveguide laser) and W_p is the effective pumping rate. Note that longitudinal pumping provides us with an extra-large interaction length and thus much higher absorption rate than transverse pumping. The terms on the right-hand side of (9) express the net stimulated emission, spontaneous emission and optical pumping. For a laser working at cw operation under constant pumping power, that is, $dW_p/dt = 0$, the inversion population density

$$n = n_2 - \frac{g_2}{g_1} n_1 \tag{11}$$

needs to be achieved and maintained at a constant value. The value of ϕ, the photon density, also needs to be maintained. Optimum REI concentration in conjunction with pumping power provides a desired n value. A stable cavity design keeps the level of ϕ, which is linearly proportional to the intensity of stimulated emission, at a high level.

Similar to polymer waveguide preparation, the Nd^{+++}/photolime gel was spin-coated on top of a substrate. The Nd^{+++} concentration was determined to be 1.03×10^{20} cm^{-3}. On standing at temperatures below 30°C, solutions containing more than 1% photolime gels become rigid through material cross-linking and exhibit rubber-like mechanical properties. This gelation process holds for both pure gel and doped gel alloy. The absorption spectrum, which determines the optimal pumping wavelengths, was experimentally confimed using a spectrophotometer. Two major peaks shown in Fig. 17(a) are in the 750 nm and 790 nm neighbourhood. The film thickness used for this measurement was 250 nm. These absorption peaks are very similar to those shown in the Nd:glass ED-2. Note that, due to the amorphous nature of the host material, that is, photolime gel, the absorption width of each peak is much wider than single crystal Nd:YAG laser. The fluorescent spectrum of Nd^{+++}:photolime gel thin film was also observed by pumping the active medium using a Ti:sapphire laser working at 790 nm. The fluorescent spectrum detected by an optical spectrum analyser is illustrated in Fig. 17(b) where a fluorescent peak centred at 1.06 μm is indicated. Note that the broadening effect due to the amorphous structure of the photolime thin film is also observed. It is equivalent to the $^4F_{3/2}$ to $^4I_{11/2}$ transition of an Nd:glass laser. A wider line increases the laser threshold since a larger population inversion is required to obtain the threshold value of amplification. However, this broadening effect has an advantage. A broader line offers the possibility of obtaining and of amplifying shorter light pulses. In addition, it permits the storage of large amounts of energy in the amplifying medium for the same linear amplification coefficient.

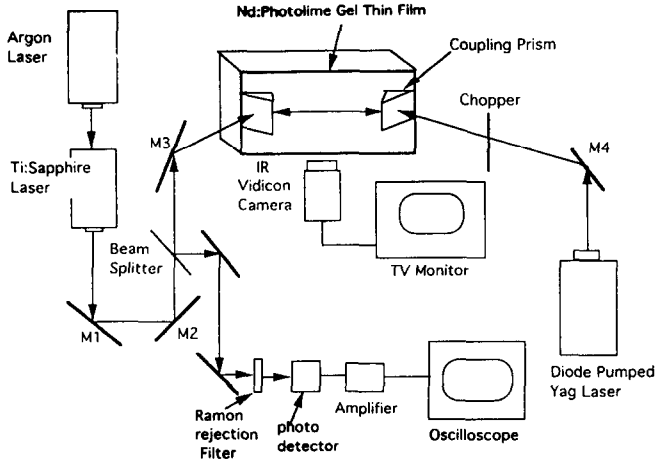

Fig. 18 Set-up for the demonstration of the graded index (GRIN) polymer waveguide amplifier

The set-up for the demonstration of a graded index (GRIN) polymer waveguide amplifier is shown in Fig. 18. The interaction length, that is, the waveguide region for two counter-propagating laser beams, is 2.2 cm. The propagation loss at 750 nm was measured to be 9.3 dB cm^{-1} which is around two orders of magnitude higher than a pure photolime gel waveguide. The pumping laser beam and the 1.06 μm Nd:YAG laser beam are both coupled into the Nd:photolime gel waveguide using the prism coupling method. The input prism coupler for 750 and 790 nm laser beams also functions as an output prism coupler for the amplified 1.06 μm laser beam. An infra-red vidicon camera is employed in the alignment process. The Nd:photolime gel medium is a planar waveguide without horizontal confinement. Therefore, the overlap between the pumping beam and the amplified laser beam (1.06 μm) plays an important role in

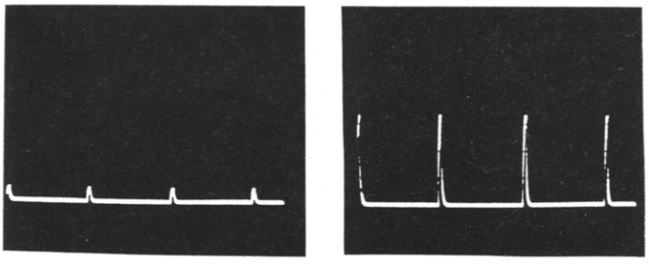

(a) Without Amplification (f=100Hz)

(b) With Amplification (f=100Hz), 8.5 dB Gain is Observed.

Fig. 19 Measured results of the graded index (GRIN) polymer waveguide amplifier; 8.5 dB gain is clearly shown at 100 Hz

achieving the maximal value of amplification. The measured gain for the demonstration shown in Fig. 18 is illustrated in Fig. 19. An 8.5 dB gain is clearly observed[50].

Polymer-based electro-optic waveguide modulator

An important characteristic of modulators and switches is the bandwidth or range of modulation frequencies over which the electro-optic material can be operated. By convention, the bandwidth of a modulator is usually taken as the difference between the upper and lower frequency responses, which is 3 dB less than the maximum modulation depth. Minimizing the switching time is important when large-scale arrays or switches and modulators are used to route optical signals over desired paths. Similarly, modulation bandwidth is a critical factor when many information channels are to be multiplexed onto the same optical beam. Thus, the usually fast switching speed and large bandwidth of waveguide switches and modulators make them particularly useful in large communications systems such as phased-array antenna.

There are two different types of electrode structures that have been realized to date. They are the lumped electrode structure and the travelling-wave. The first regards the modulator as a capacitor and usually has a 50 Ω resistance in parallel with the device. The second type treats the electrode pair as a continuation of a transmission line. The 3 dB bandwidth of the second type is usually higher than the first. The bandwidth of the lumped electrode-type is limited by the RC constant, whereas the bandwidth of the travelling-wave electrode-type is constrained by the difference of the effective indices of the optical guided wave and the microwave and the interaction length.

A graded index polymer waveguide modulator based on current injection has been previously reported[51]. The polymer-based electro-optic device reported here provides wider modulation bandwidth due to its small walk-off when compared with $LiNbO_3$ and GaAs counterparts. The device structure is shown in Fig. 20[52]. A channel waveguide array is made using the method described earlier. The HeNe laser beam coupled into the channel waveguide array is circular polarized. Mode conversion is activated through the electric field induced phase velocity difference between TE (transverse electric) and TM (transversde magnetic) modes. A third section of the waveguide

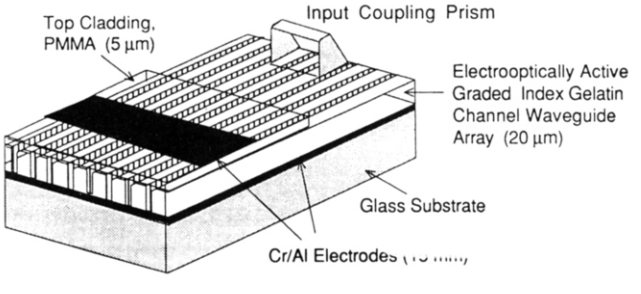

Fig. 20 Photolime polymer-based electro-optic mode converter[52]

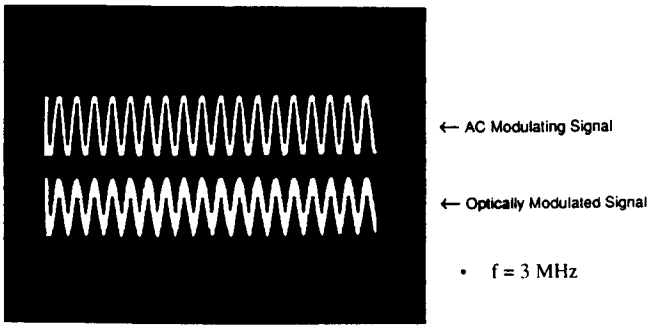

Fig. 21 Low frequency modulated signal with 12 dB modulation bandwidth and the applied voltage is 10 V

with aluminium cladding is also shown in Fig. 20. The TM wave has a much stronger propagation loss in this section. The modulation effect is represented by

$$V_\pi = \frac{3d}{L}\frac{\lambda}{2n^3\gamma_{33}} \tag{12}$$

The combination of these effects results in a modulation depth of 12 dB with an applied voltage of $10\,V_{p-p}$. The result is shown in Fig. 21. Emitter-coupled logic (ECL) and TTL compatible electrical-to-optical digital signal conversion can also be generated when appropriate logic input is provided.

A photolime polymer-based travelling wave electro-optic Mach-Zehnder interferometer with 40 GHz electrical bandwidth was reported recently[53]. This device structure was based on the χ^2 non-linear polymer described earlier. It is clear from the measured result depicted in Fig. 22 that the modulation bandwidth can be higher than 40 GHz. The data shown is limited by the availability of the microwave source.

Improvement of the performance relies on a new procedure and material combination through which the performance of each individual integrated optical device is upgraded. Polymer-based guided wave devices provide both architectures (due to the GRIN characteristic) and device level improvements not achievable through conventional GaAs- and $LiNbO_3$-based devices.

The major stumbling block for polymer-based electro-optic devices is their relatively short lifetime, usually weeks or months, due to the relaxation of the polarization density. χ^2 non-liner polymers are

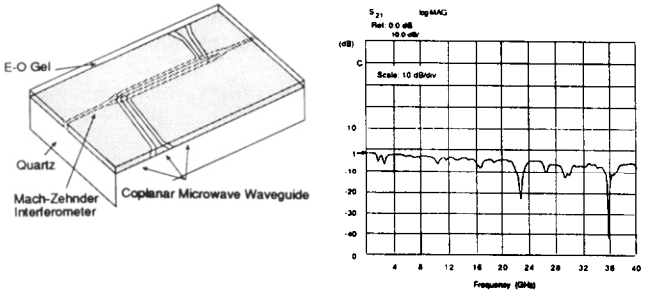

Fig. 22 A photolime gel polymer-based travelling wave electro-optic Mach-Zehnder interferometer with measured 40 GHz electrical bandwidth

prepared by either the guest/host mixture method or side chain polymerization or cross-linking. If a strong crosslink can be generated after the formation of a non-linear polymer, long-term stability of the polymer matrix can be achievable.

Fan-out density and optical interconnection

The techniques used to develop the 12-channel demultiplexer shown in Fig. 10 can also be used to create 1-to-N fan-out elements for optical interconnection. Such elements will undoubtedly require high efficiencies and low channel crosstalk. Improvements in diffraction efficiency can be expected through careful control of the phase grating parameters, while enhancements in crosstalk figures will depend upon the ability to achieve minimal angular overlap between adjacent fan-out directions. The modulation index of the polymer film, and its dependence on exposure dosage will ultimately determine the maximum number of phase gratings that can be exposed within a given region of the polymer microstructure waveguide (PMSW), as well as the overall grating efficiency.

Using coupled mode theory, as it applies to a lossless step index waveguide medium containing slanted phase gratings[54], the diffraction efficiency, and the angular and wavelength selectivities, can be determined, as a function of grating and waveguide parameters, including the interaction length d, index modulation Δn and overlap integral, for the TE mode of the waveguide. The diffraction efficiency is given by the expression

$$\eta = \frac{4\kappa^2(\hat{r}\cdot\hat{s})^2}{\frac{C_r}{C_s}\vartheta^2 + 4\kappa^2(\hat{r}\cdot\hat{s})^2} \times \sin^2\left[\frac{1}{2}\left(\frac{\vartheta^2}{C_s^2} + \frac{4\kappa^2(\hat{r}\cdot\hat{s})^2}{C_r C_s}\right)^{1/2} d\right] \quad (13)$$

where

$$C_r = \frac{\beta_{mz}}{\beta_m}$$

$$C_s = \frac{\sigma_z}{\beta_l}$$

$$\vartheta = \frac{\beta_l^2 - \sigma^2}{2\beta_l} \quad (14)$$

$$\vec{\sigma} = \vec{\beta}_m + \vec{K} \quad (15)$$

$$\kappa = \frac{2\pi^2}{\lambda^2}\int_{-\infty}^{\infty} n_0(y)\,\Delta n(y) E_m(y) E_l(y)\,dy \quad (16)$$

Here, $\hat{r}$ and $\hat{s}$ are the unit polarization vectors, β_m and β_l are the propagation constants of the incident and diffracted guided modes, and $\vec{K}$ is the grating wavevector, respectively. We use σ as the propagation constant of the diffracted mode, and introduce a small dephasing constant ϑ, as in (14), to characterize the angular and wavelength selectivities of our planar hologram. The Bragg condition is given in (15) which can be used to determine the diffraction angle and the constant σ. Equation (16) gives the coupling strength, which depends on the overlap between the incident guided model $E_m(y)$, the diffracted guided model profile $E_l(y)$ and the grating index profiles, $n_0(y)$ and $\Delta n(y)$. $E_m(y)$ and $E_l(y)$ satisfy the orthogonality relationship

$$\int_{-\infty}^{\infty} E_m(y)E_l(y)\,dy = \frac{\delta_{m,l}}{\beta_m} \quad m, l = 0, 1, 2, \ldots \quad (17)$$

For the calculation, it is assumed that there is complete overlap between the guided mode and the index perturbation, and that the modulation index for each individual grating has a value of $\Delta n \sim 0.01$. We note that the effects of having a finite laser beam width and a graded refractive index profile have not been accounted for in the present analysis. Additional losses that might have been introduced during the polymer thin film sensitization process have similarly been neglected. As expected, the diffraction efficiency of the induced transmission hologram undergoes a periodic transition between a maximum and a minimum value, as the diffraction angle is changed. The diffraction efficiency of each individual waveguide hologram can be improved by changing the exposure dosage during the recording process[55]. The modulation index, as a function of exposure time T_i for the ith hologram, can be determined from the expression

$$\Delta n_i = \left(\Delta n_{max} - \sum_{j}^{i-1}\Delta n_j\right)(1 - e^{-\gamma E T_i}) \quad (18)$$

where γ is a sensitivity constant associated with the DCG material, E is the exposure intensity of the laser beam, Δn is the modulation index value achieved for each exposure, and Δn_{max}, the maximum index modulation that can be achieved in DCG holographic material, assumes a value of 0.2. The exposure of the ith hologram is therefore dependent on the exposure parameters of all previously exposed $(i-1)$ holograms. Based upon the gelatin waveguide and exposure parameters used in our experiments, we

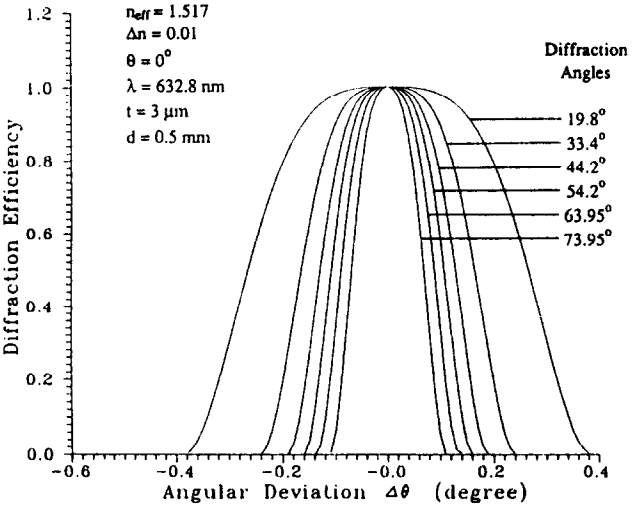

Fig. 23 Angular selectivity for TE guided wave at different diffraction angles

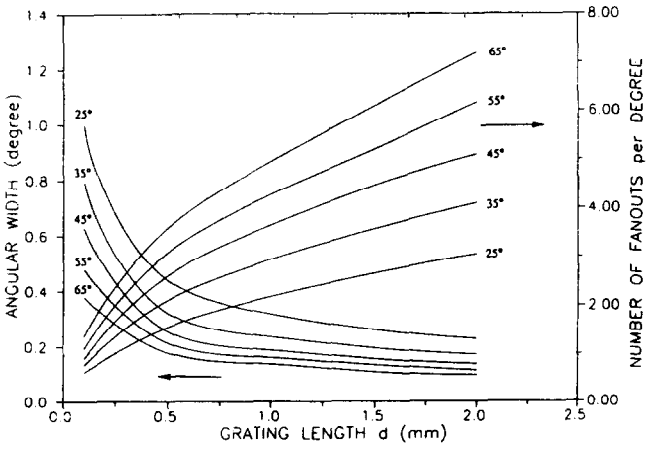

Fig. 24 Angular bandwidth and fan-out density, plotted as a function of grating interaction length d. Mode effective index $N_{eff} = 1.517$, centre wavelength $\lambda = 0.6328\ \mu m$, and waveguide thickness $t = 3\ \mu m$ were used in the calculation

estimate that a maximum of ~300 multiply exposed gratings can be fabricated before the modulation index response of the locally sensitized PMSW begins to saturate.

The angular selectivity of our device structure, calculated using (13)–(17), is shown in Fig. 23. The diffraction angles are chosen such that all curves are normalized to unity for fixed index modulation Dn. To achieve maximum efficiency at other diffraction angles, Δn can be adjusted. The dependence of the angular width, and fan-out channel density, as a function of grating interaction length and diffraction angle, are shown in Fig. 24. In this case, the modualtion index for each individual waveguide hologram was fixed at a value of 0.01. A mode effective index $N_{eff} = 1.517$, a waveguide thickness $t = 3\ \mu m$, and a centre wavelength $\lambda = 632.8$ nm were also used in the calculation. As seen in Fig. 24, a decrease in angular bandwidth can be achieved by comparison with waveguide-based devices, where light propagation occurs within the plane of the waveguide layer over large distances, the smaller interaction lengths (<60 mm) of bulk holographic 1-to-N fan-outs and WDM devices actually preclude the achievement of very high channel densities. Based upon the above calculations, a maximum channel density of ~7 fan-outs per degree can be expected, for a grating interaction length of 2 mm and a Bragg diffraction angle of 65°. We note that, by virtue of the polymer material and waveguide geometry, the interaction length can vary from mm to cm in dimension. Hence, the modulation index needed to form a high efficiency deflection device in PMSWs is smaller than in corresponding bulk holographic devices. For example, an interaction length of 0.5 mm would require an modulation index of only $\sim 4 \times 10^{-4}$ in order to achieve 100% diffraction efficiency at an angle of 30°. Since the fan-out density is largely dependent upon the maximum modulation index of the material, DCG is expected to outperform other photorefractive materials, such as Fe-doped $LiNbO_3$ and SBN, which can achieve maximum modulation indices that are, at best, 2–3 orders of magnitude smaller.

Reliability test

To evaluate further the reliability of waveguide devices reported here, semi-hermetically sealed samples were made using EPO-TEK 353ND epoxy. The advantages of using this epoxy include its characteristics of curing at lower temperature and surviving at a higher temperature, low cost and easy handling. The temperature stability results of an unslanted grating hologram under hermetic sealing using Aremco-Bond 631 have been demonstrated. The long drying time and serious out-gas problem have limited the potential of using Aremco-Bond 631 for our hermetic sealing purposes. Thus, our attention has switched to alternative adhesive materials. EPO-TEK 353ND epoxy from Epoxy Technology has been found to be an excellent candidate for our purposes.

EPO-TEK 353ND has a flexural strength of 10 600 psi, a compressive strength of 20 200 psi, and a lap shear strength for glass-to-glass bonding of 1180 psi. It has excellent moisture resistance and temperature stability range. It is important to note that the curing time for this epoxy is very short; 1 minute at 150°C or 2 minutes at 120°C. In case there is some minor out-gas during this short drying period, the box can always be flushed simultaneously during drying using N_2 gas and then the purging hole can be sealed. It is assumed that this does not generate serious out-gas problems due to the small volume of epoxy. In fact, the waveguide device was not damaged by the direct contact of this epoxy. Damageable chemical reactions between the waveguide hologram and the epoxy or its out-gas are anticipated. During the box fabrication period, the holograms are continuously baked between 80°C to 120°C; this eliminates the potential for moisture penetration or absorption by the hologram. This procedure helps to stabilize the hologram prior to encapsulation.

Various baking temperatures are used to test the device stability under sealing. For each temperature testing, we use three different PMSW holograms including an unslanted grating hologram used for our substrate fan-out optical interconnects[55], a slanted Littrow grating hologram and a Lippmann grating hologram. The results are general and applicable to all other types of microstructure waveguide devices.

The diffraction efficiency, diffraction angle, transmission characteristic, optical density (OD), and centre wavelength, if applicable, to each corresponding grating type, are tested before and after each temperature treatment. The diffraction efficiency and diffraction angle are measured using an HeNe laser of 632.8 nm wavelength. Reproducible results in optical density, transmission bandwidth, diffraction efficiency, and the diffraction angle are found in a Littrow grating of up to 180°C. The shift in OD peak wavelength to lower wavelength values of ~18 and 24 nm occurs after baking at 160°C and 180°C, respectively. The slightly larger fluctuation was found to be caused by a relatively large hologram non-uniformity. The shift of OD

Table 4. Grating response after baking in oven at 180°C for 2 hours

Littrow grating hologram							
Baking cycle	Duration	Temp.	Transmission n bandwidth	OD	OD peak λ	Diffraction efficiency y	Diffraction angle
Before bake			145 nm	2.83	642 nm	88.4%	11.8°
1	1 hour	180°C	140 nm	2.6	620 nm	88.5%	11.86°
2	1 hour	180°C	129 nm	2.57	610 nm	86.5%	11.83°

Lippmann grating hologram					
Baking	Duration	Temperature	Transmission bandwidth	OD	OD Centre λ
Before bake			140 nm	1.55	660 nm
1	1 hour	180°C	130 nm	2.84	630 nm
2	1 hour	180°C	140 nm	3.45	628 nm

centre wavelength to lower wavelength values is consistent with the results of the Littrow grating due to the possible emulsion shrinkage in the depth direction which reduces the grating fringe spacing.

The same temperature cycling test has been performed on both transmission and reflection holograms at 120°C, 140°C, 160°C and 180°C. Table 4 shows the results of a temperature treatment at 180°C. The Littrow grating shows a better response than the Lippmann grating. This may be explained by the better hologram preparation condition for the Littrow grating. The stabilization of holograms, within a few baking cycles, suggests that all holograms should be pre-baked before using them for practical applications. Pre-baking at similar to, or higher than, application temperature is required.

Military specifications require a stability between −62°C to 125°C. We passed this requirement on the positive temperature side. On the negative temperature side, our experiments were concluded at −66°C, −100°C and a liquid nitrogen temperature of −196°C. There were no observable changes after a one hour treatment at −66°C and −100°C and −196°C, respectively. Figure 25 shows the transmission and optical density plots for a Lippmann hologram before and after treatment at −196°C. Stable results for other holograms have also been observed. At −196°C, considerable care is needed to submerge the holograms into the liquid nitrogen. Submerging the holograms too fast will result in a temperature shock, which will, in turn, either damage the hologram, the hermetically-sealed box, or both. The experimental result has proven that the hermetically-sealed hologram can survive at liquid nitrogen temperatures.

All of our polymer-based active and passive device samples have failed after baking at 200°C. An irreversible phase transition occurred at this temperature. Partial damage and complete damage have been found after 10 minutes and 1 hour bakings, respectively.

The EPO-TEK 353ND epoxy has excellent moisture resistance. As specified, its weight increased by 0.03% after 7 days at a 96% humidity level. After submerging the boxed holograms in water for two days at room temperature, no observable damage occurred.

If properly prepared, waveguide devices, including our unslanted grating hologram, can survive temperatures between −196°C to +180°C under hermetic sealing if they are internally filled with dry N_2 gas. Survival at −196°C, the liquid nitrogen temperature, is also anticipated. In addition, the two-day water test showed no changes to the photolime gel-based waveguide devices.

Further applications

Many far-reaching applications can be realized based on the polymer microstructure waveguide (PMSW) technology. Basically, the PMSW we proposed and then developed in this program will find its suitability in all optical and electro-optic systems that involve microstructure waveguides. The capability of locally sensitizing and selectively doping the PMSW with the desired materials provides us with a new method to

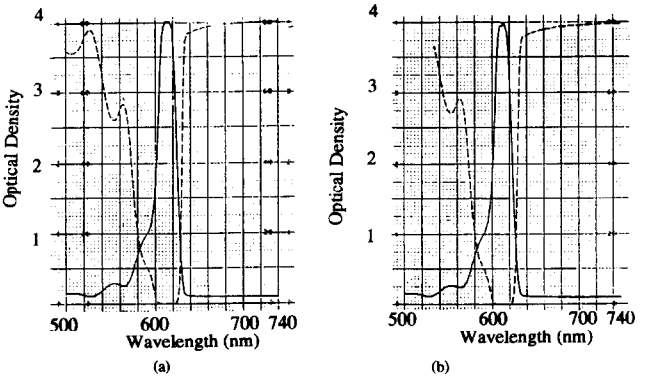

Fig. 25 Response in transmission (dashed curve) and optical density (solid curve) of a Lippmann Hologram (a) before and (b) after one hour temperature treatment at −196°C

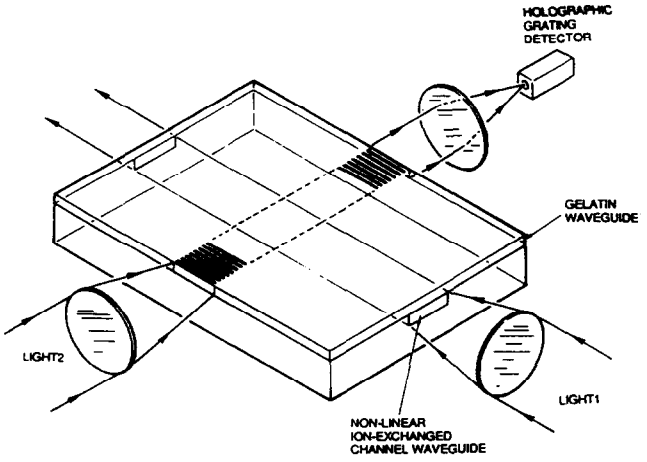

Fig. 26 Non-linear all-optical switch based on PMSW on non-linear substrates

develop passive and active optoelectronic systems. Some of the more highly plausible applications are described further in this section.

Where the speed and the number of fan-outs increases, there is a need to employ optical interconnects on the backplane to perform board-to-board interconnection. We have already concluded that a PMSW can be constructed on any smooth surface including insulators, semiconductors and conductors. As a result, PMSWs are an attractive alternative to realizing the backplane interconnection. The PMSW is deposited on the backplane which holds the layers of IC boards. If the interconnectivity and parallelism needs to be increased further, several integrated PMSW backplanes can be added on the same board. Optical components such as laser diodes, photodetectors, and multiplexed holograms can be interpreted onto the same PMSW backplane to transmit, route and receive the optical signals.

Non-linear all-optical switch

The capability of constructing PMSWs on any surface and of selectively doping the PMSW provides us with some alternatives to build active optical and electro-optical devices. Figure 26 shows an optical switch/modulator. In this case, the substrate material needs to be a non-linear material with a large $\chi^{(3)}$; for example, semiconductor-doped glass commercially available from Corning. The PMSW on top

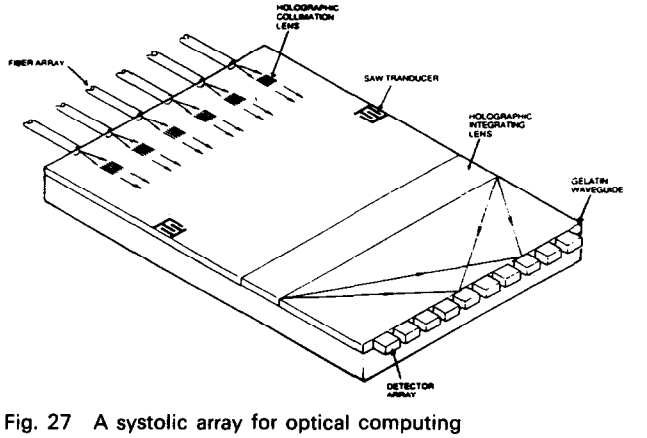

Fig. 27 A systolic array for optical computing

of the non-linear material is locally sensitized with ammonia dichromate. Two gratings which function as the rejection filter are accordingly formed. A single-mode guided wave Fabry-Perot etalon is created. Light is the pumping beam creating the non-linear effect. The substrate index of the PMSW is thus modulated. This effect changes the effective index of the guided wave of PMSW and, therefore, the optical path, OP, which is defined as

$$\mathrm{OP} = L \cdot N_{\mathrm{eff}} \tag{19}$$

where L is the physical length of the PMSW. The maximum transmission of a Fabry-Perot etalon occurs when

$$\frac{2 \cdot \mathrm{OP}}{\lambda} = m \tag{20}$$

where λ is the wavelength of the signal carrier and m is an integer. Since

$$\lambda \ll \mathrm{OP} \tag{21}$$

holds for a real device, a small change of the intensity of the pumping power will drastically change the throughput of the signal wave. Another possibility for active device application is to dope selectively the PMSW with non-linear materials with large $\chi^{(2)}$ or $\chi^{(3)}$ and then an optical device or an electro-optic device can be easily built.

Systolic arrays for optical computing

Vector and matrix multiplication can be implemented by integrating passive and active devices such as waveguides, grating lenses, and acousto-optic Bragg cells on the same substrate. A systolic array is shown in Fig. 27. All devices can be built on top of the PMSW. Acousto-optic and piezoelectric effects of PMSWs need to be studied further to realize such a system application. By integrating a large array of holographic gratings, a large-dimension matrix and vector multiplication can be produced and performed. Realization of optical communications, signal processing, and computing functions in a PMSW is certainly the major application of integrated optics. Previously, such computing and signal processing modules only existed in $LiNbO_3$. The capability of applying PMSW to various substrates and the reproducibility of the experiments provide a promising future for such architectures on different electro-optic materials.

PMSW itself is transparent over a wide range of the optical spectrum. Accordingly, the PMSW itself functions as a good optical path to route optical waves with various wavelengths ($\sim 0.3\,\mu$m to $\sim 2.7\,\mu$m). A high density wavelength division multiplexing and demultiplexing device based on PMSW technology and multiplexed holograms is feasible. Integration of holographic lenses and highly multiplexed Bragg holograms into PMSWs is shown in both the transmitter and the receiver. Since the refractive index modulation of DCG can be as high as 0.2, a large number of gratings can be multiplexed

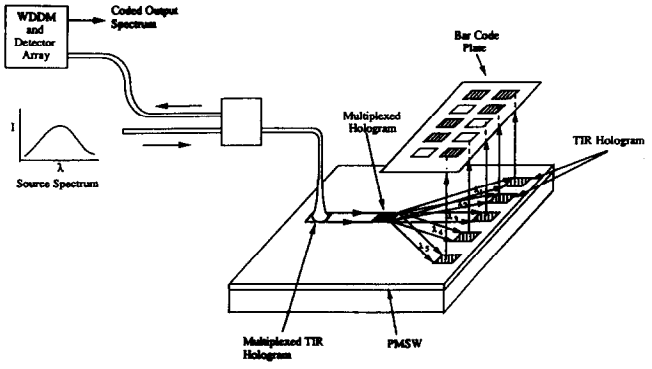

Fig. 28 Schematic illustration of broadband energy being transmitted through a WDM system to a fibre sensor

on the same holographic emulsion. Local area networks, highly parallel computer interconnections and long distance, wide-band communications are some of the areas in which the PMSW-based WD(D)M will find its use.

Position sensor

Recently, fibre-optic sensors based on wavelength division multiplexing (WDM) techniques have been a major area of interest. By using WDM techniques, rotary and linear position sensing, rotary speed sensing, and pressure and temperature sensing information is provided. WD(D)M devices are used to create a chromatically dispersed strip of light, which can either be an LED or a laser diode array. The dispersed light is then focused onto the code tracks which contain binary information (that is, transmission, 0; reflection, 1). Different binary codes correspond to different sensed parameters. The detected optical signal is coupled back into a fibre through the same WDM device. The topology of this sensor system is shown in Fig. 28. The PMSW WDM we propose here is an outstanding device for this application. For example, the four-channel WDM we demonstrated can be used as a linear or rotary position sensor for 16 different positions. Each individual position is identified by different binary codes. Figures 29(a) to (c) represent (1, 0, 0, 1) (1, 1, 0, 0) and (1, 0, 1, 1), respectively.

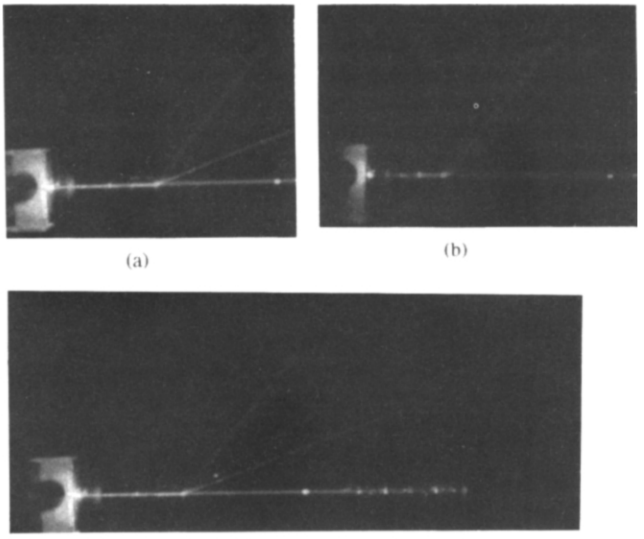

Fig. 29 Four big position sensors (a) (1, 0, 0, 1), (b) (1, 1, 0, 0), (c) (1, 0, 1, 1)

Conclusions

In this paper I have reported on the research and development results of the photolime gel-based passive and active guided wave devices. High density linear and curved channel waveguide arrays, electro-optic modulator and modulator arrays, highly multiplexed waveguide holograms for wavelength division demultiplexing and optical interconnects and waveguide lenses, rare earth ion doped polymer waveguide amplifiers have been described. A single-mode linear channel waveguide with a device packing density of 1250 channels cm^{-1} was achieved. A 12-channel wavelength division demultiplexer working at 830, 840, 850, 860, 870, 880, 890, 900, 910, 920, 930 and 940 nm wavelengths is also described in this paper. A polymer-based electro-optic travelling wave modulator with 40 GHz electrical bandwidth is detailed. A rare earth ion doped polymer waveguide amplifier working at 1.06 μm with 8.5 dB optical gain is also reported.

Laminated guided wave devices demonstrated outstanding temperature stability from -196°C to $+180$°C. Humidity tests also showed the survivability of the devices. Table 1 summarized the demonstrated features of the polymer-based guided wave passive and active devices with III-V and $LiNbO_3$ as references. All the devices listed in Table 1 can be substituted with the reported technologies. Other devices, such as highly multiplexed waveguide holograms, large coating areas and compression-moulded optical channel waveguides can only be achieved by the polymeric material reported here. These device characteristics make polymer-based guided wave devices much more suitable for optoelectronic interconnection applications, such as optical backplane, wafer scale optical interconnects and multi-chip module optical interconnects.

Acknowledgements

This research is partially sponsored by SDIO/IST, Army SDC, Army Research Lab, DARPA, WPAFB, Army Research Office, NSF, DOE, NASA and the faculty start-up funding of the School of Engineering at the University of Texas, Austin. Assistance from research scientists, engineers and technicians involved in this research is also acknowledged and their names can be found in the references.

References

1 **Man, H.T., Chiang, K., Haas, D., Teng, C. C. Yoon H.N.** Polymeric materials for high speed electrooptic waveguide modulators, *Proc SPIE* **1213** (1990) 13
2 **McDonach, A., Copeland, A.** Polymeric guided wave optics, *Proc SPIE* **1177** (1989) 67
3 **Cross, G.H., Donaldson, A., Gymer, R.W., Mann, S., Parsons, N.J., Haas, D. R., Man, H. T., Yoon, H.N.** Polymeric integrated electrooptic modulator, *Proc SPIE* **1177** (1989) 79
4 **Haas, D., Yoon, H., Man, H.T., Cross, G., Mann, S., Parsons, N.** Polymeric electrooptic waveguide modulator: materials and fabrication, *Proc SPIE* **1147** (1989) 222

5 **Beeson, K.W., Horn, K.A., McFarland, M., Nahata, A., Wu, C., Yardley, J.T.** Polymeric materials for guided-wave devices, *Proc SPIE* **1337** (1990) 1

6 **Lytel, R., Lipscomb, G.F.** Nonlinear and electrooptic organic devices, *Optical Nonlinearities in Organic Materials: Fundamentals and Device Applications*, eds. P.N. Prasad and D.R. Ulrich, Plenum Press, New York, (1988) 415

7 **Hacker, N.P., Welsh, K.M.** Photochemistry and fluorescence spectroscopy of polymeric materials containing triphenylsulfonium salts, IBM Research Report, RJ 8278 (75639), Chemistry (1991)

8 **Sullivan, C.T., Husain, A.** Guided-wave optical interconnects for VLSI systems, *Proc SPIE* **881** (1988) 172–176

9 **Sullivan, C.T., Booth, B.L., Husain, A.** Polymeric waveguide, *IEEE Circuits and Devices* **27** (1992)

10 **Chen, R.T.** Optical interconnects: a solution to very high speed integrated circuits and systems, *Proc SPIE* **1374** (1990) 20

11 **Chen, R.T., Lu, M., Robinson, D., Wang, M.R., Savant, G., Jannson, T.** Guide wave planar optical interconnections using highly multiplexed polymer waveguide holograms, *J Lightwave Technology* **10** (1992) 888

12 **Chen, R.T., Wang, M.R., Sonek, C., Jannson, T.** Optical interconnection using polymer microstructure waveguides, *Opt Eng* **30** (1991) 622

13 **Zyss, J.** Nonlinear organic materials for integrated optics, a review, *J Moleculkar Electron* **25** (1985)

14 **Booth, B.L.** Low loss channel waveguides in polymers, *IEEE J Lightwave Technol* **7** (1989) 1445

15 **Thackara, J.I., Lipscomb, G.F., Stiller, M.A., Ticknor, A.J., Lytel, R.** Poled electrooptic waveguide formation in thin film organic media, *Appl Phys Lett* **52** (1988) 1031

16 **Sullivan, C.T.** Optical waveguide circuits for printed wire-board interconnections, *Proc SPIE* **994** (1988) 14

17 **Franke, H., Crow, J.D.** Optical waveguiding in polyimide, *Proc SPIE* **651** (1986) 102

18 **Herman, W.N., Rosen, W.A., Sperling, L.H., Murphy, C.J., Jain, H.** A high Tg nonlinear optical polymer: Poly(N-MNA Acrylamide), *Proc SPIE* **1560** (1991) 225

19 **Smith, B.A., Herminghaus, A.J., Swalen, J.D.** Electrooptic coefficients in electric field poled polymer waveguides, *Proc SPIE* **1560** (1991) 400

20 **Yankelevich, D., Knoesen, A., Eldering, C.A., Kowel, S.T.** Reflection-mode polymeric interference modulator *Proc SPIE* **1560** (1991) 406

21 **Chen, R.T.** Graded index cross-link induced linear and curved channel waveguide array for high density optical interconnects, *Appl Phys Lett*, November (1992)

22 **Chen, R.T.** Polymer-based waveguide devices for optical interconnects, Final Report to Army Strategic defence Command and Strategic Defence Innitiative Office, Contract No. DASG60-90-C-0047 (1992)

23 **Chen, R.T.** Polymer-based guided wave devices and their applications. Invited Talk at the Symposium on Polymeric Materials for Electrooptic Applications, Organized by The Rank Prize Funds, London, 7–10 December (1992)

24 **Chen, R.T., Phillips, W., Pelka, D., Jannson, T.** Integration of polymer waveguide with GaAs, $LiNbO_3$, glass and aluminum to provide massive fanout optical interconnect for computing, Postdeadline Paper, IEEE/OSA Topical Meeting on Optical Computing, PD-1, Post conference edition, **9** (1991) 425

25 **Chen, R.T., Wang, M., Jansson, T.** Polymer microstructure waveguide on BeO and Al_2O_3 substrates for optical interconnection, *Appl Phys Lett* **56** (1990) 709

26 **Chen, R.T., Wang, M.R., Jansson, T.** Intraplane guided wave massive fanout optical interconnects, *Appl Phys Lett* **57** (1990) 2071

27 **Chen, R.T., Phillips, W., Pelka, D., Jannson, T.** Gelatin waveguides in conjunction with integrated holographic optical elements in GaAs, $LiNbO_3$, glass and aluminum substrates for optical signal processing, *Opt Lett* **14** (1989) 892

28 **Chen, R.T.** Gelatin waveguide for optical interconnection, *Proc SPIE* **1151** (1989) 60

29 **Chen, R.T.** Polymer microstructure waveguides on various substrates for optical interconnection and communication, *Proc SPIE* **1213** (1991) 100

30 **Chen, R.T.** Cross-link induced linear and curved polymer channel waveguides for high density optical interconnects, *Proc SPIE* **1774** (1992) 10

31 **Chen, R.T., Lu, H., Jannson, T.** Highly multiplexed graded index polymer waveguide hologram for near-infrared eight-channel wavelength division demultiplexing, *Appl Phys Lett* **59** (1991) 1144

32 **Hocker, B., Burns, W.K.** Mode dispersion in diffused channel waveguides by effective index method, *Appl Opt* **16** (1977) 113

33 **Marcatili, E.A.J.** Dielectric waveguide and directional coupler for integrated optics, *Bell Syst Tech J* **48** (1969) 2071

34 **Chen, R.T.** Microprism array for large-scale wide-band optical interconnection for optoelectronic systems. Final Report to ISDO/IST and Army Research Office, Cont. No. DAAL03-91-0030 (1992)

35 **Chen, R.T., Tsai, C.S.** Thermally annealed single-mode proton-exchange channel waveguide cutoff modulator, *Opt Lett* **11** (1986) 546

36 **Marcatili, E.A.J.** Bends in optical dielectric guides, *Bell Syst Tech J* **48** (1969) 2162

37 **Marcatili, E.A.J., Miller, S.E.** Improved relations describing directional control in electromagnetic waveguidance, *Bell Syst Tech J* **48** (1969) 2161

38 **De. Giacomo, J.** (Ed) *Digital Bus Handbook*, (McGraw–Hill, New York (1990) and **Heath, S.** *VMEbus User's Handbook* CRC Press, Inc., Florida (1989)

39 **Chen, R.T., Lu, H., Robinson, D., Sun, Z., Jannson, T., Plant, D., Fetterman, H.** 60 GHz board to board optical interconnection using polymer optical buses in conjunction with microprism couplet, *Appl Phys Lett* **60** (1992) 536

40 **Chen, R.T., Lu, H., Jansson, T.** Eight-channel wavelength division demultiplexer using multiplexed GRIN polymer waveguide hologram. Post-deadline paper for OSA/IEEE Topical Meeting on GRIN Optical Systems, PD2-1 (1991)

41 **Chen, R.T., Lu, H.** Polymer-based 12-channel single-mode wavelength division multiplexer on GaAs substrates, *Proc SPIE* **179** (1992) 44

42 **Lubensky, T.C., Pincus, P.A.** Supermolecules, *Phys Today* Oct 44 (1984)

43 **Williams, D.J.** (Ed.) *Nonlinear Optical Properties of Organic and Polymeric Materials* ACS Symposium Series, 233, Washington, DC (1983)

44 **Ho, Z.Z., Chen, R.T., Shih, R.** Electrooptic effect in gelatin-based nonlinear polymer, *Proc SPIE* **1774** (1992) 29 and Electro-optic phenoma in gelatin-based poled polymer *Appl Phys Lett* **61** (1992) 4

45 **Layne, C.B., Weber, M.J.** Multiphonon relaxation of rare-earth ions in beryllium-fluoride glass, *Phys B* **16** (1977) 3259–3261

46 **Gapontsev, V.P., Matitsin, S.M., Isineev, A.A., Kravchenko, V.B.** Erbium glass laers and their applications, *Opt and Laser Technol* **14** (1982) 189–196

47 **Miniscalo, W.J.** Erbium-doped glasses for fiber amplifiers at 1500 nm, *IEEE J Lightwave Technol* **9** (1991) 234

48 **Armitage, J.R.** Three-level fiber laser amplifier: a theoretical model, *Appl Opt* **27** (1988) 4831–4836

49 **Wang, M.R., Chen, R.T., Sonek, G., Jansson, T.** Waveguide division demultiplexing device on polymer microstructure waveguide, *Opt Lett* **15** (1992) 363

50 **Chen, R.T., Ho, Z.Z., Robinson, D.** Graded index polymer waveguide amplifier. Postdeadline Paper, *Proc SPIE* **1774** (1992) 39

51 **Chen, R.T., Sadovnic, L., Jannson, T., Jannson, J.** Single-mode polymer waveguide modulator, *Appl Phys Lett* **57** (1991) 2071

52 **Shih, R., Chen, R.T., Ho, Z.Z.** Travelling wave polymer waveguide modulator using coplanar electrode structure, *Proc SPIE* **1774** (1992) 11

53 **Shih, R., Chen, R.T., Ho, Z.Z.** Traveling-wave electrooptic polymer waveguide modulator using coplanar electrodes, *Proc SPIE* **1794** (1992) 53

54 **Chen, R.T., Lu, H., Jannson, T.** Highly multiplexed graded index polymer waveguide hologram for near infrared eight-channel wavelength division demultiplexing, *Appl Phys Lett* **59** (1992) 1144

55 **Chen, R.T., Wang, M. R., Jannson, T.** Intra-plane guided wave massive fanout optical interconnects, *Appl Phys Lett* **57** (1990) 2071